Distribution Category:
LMFBR—Components: Base
Technology (UC-79k)

ANL-84-82

ANL--84-82

DE85 004829

ARGONNE NATIONAL LABORATORY
9700 South Cass Avenue
Argonne, Illinois 60439

AVOIDING LEAKAGE FLOW-INDUCED VIBRATION BY A TUBE-IN-TUBE SLIP JOINT

by

T. M. Mulcahy

Components Technology Division

DISCLAIMER

October 1984

CONTENTS

		Page
ABSTRACT		7
I.	INTRODUCTION	7
II.	TEST FACILITY	11
III.	TEST DEFINITION	14
IV.	INSTRUMENTATION	15
V.	STRUCTURAL CHARACTERIZATION	17
VI.	INSTABILITY CONDITIONS	21
VII.	FLOW DAMPING	24
VIII.	FLOW EFFECTS ON MODAL FREQUENCIES	29
IX.	PRESSURE DIFFERENCE	33
X.	ECCENTRICITY TEST	33
XI.	CONCLUSIONS	35
ACKNOWLEDGMENTS		36
REFERENCES		37

FIGURES

		Page
1	Leakage Flow Geometries.....	8
2	CRBR Shroud Tubes Slip Joint.....	10
3	Leakage Flow-induced Vibration Test Facility.....	12
4	Slip Joint.....	13
5	Electromagnetic Exciters and Intervening Bar Magnet in Calibration Fixture.....	19
6	Instability Map for Top-to-Bottom Flow where First Mode ζ_1 (%) = 0.5, □ ; 2.2, ▽; 3.3, △ ; 6.6 ○ . The Solid Symbols Indicate Instability in the Second Mode: $f_2 \cong 21$ Hz, $\zeta_2 = 0.3$. The Solid Line (——) Bounds Stable Regions.....	23
7	Variation in First-mode Damping with Top-to-Bottom Flow for (a) H/D = 0.18 and (b) H/D = 0.55 where L/D = 0.28, ○; 0.46, □ ;0.55, ▽ ; 0.64, ● ; 0.91, △	25
8	Variation in First-mode Damping with Top-to-Bottom Flow for H/D = 0.73 and L/D = 0.28, ○ ; 0.46, □; 0.55, ▽; 0.64, ● ; 0.91, △	26
9	Variation in First-mode Damping with Top-to-Bottom Flow for H/D = 1.09 and L/D = 0.28, ○; 0.46, □ ; 0.55, ▽; 0.64, ● ; 0.91, △	27
10	Variation in First-mode Damping with Bottom-to-Top Flow for (a) H/D = 0.18 and (b) H/D = 1.09 where L/D = 0.28, ○; 0.46, □; 0.55, ▽ ; 0.64, ● ; 0.91, △	30
11	Variation in First- and Second-mode Frequencies for (a) Top-to-Bottom Flow and (b) Bottom-to-Top Flow where H/D = 0.18 and L/D = 0.28, ○; 0.46, □; 0.55, ▽; 0.64, ● ; 0.91, △	31
12	Variation in First- and Second-mode Frequencies for (a) Top-to-Bottom Flow and (b) Bottom-to-Top Flow where H/D = 1.09 and L/D = 0.28, ○; 0.46, □; 0.55, ▽ ; 0.64, ● ; 0.91, △	32
13	Pressure Differences for Flow in Both Directions, H/D = 0.18, and L/D = 0.28, ○; 0.46, □ ; 0.55, ▽; 0.64, ● ; 0.91, △	34

TABLES

		Page
1	Instrumentation Used in Slip Joint Test.....	16
2	Fundamental Frequencies and Structural Damping without Slip Joint Submerged.....	20
3	First-mode Frequency, and Structural Damping, for Different Engagement Lengths, Damping Ring Heights, and No Flow.....	22

NOMENCLATURE

NOMENCLATURE

D	Raised diameter of slip joint
f_i	Frequency in ith mode
H	Height of damping rings
L	Engagement length
PH	Pad height
PW	Pad width
W	Annular gap between tubes
W'	Annular gap at constriction
ζ_i	Critical damping percentage in ith mode

AVOIDING LEAKAGE FLOW-INDUCED VIBRATION BY A TUBE-IN-TUBE SLIP JOINT

by

T. M. Mulcahy

ABSTRACT

Parameters and operating conditions (a stability map) were determined for which a specific slip-joint design did not cause self-excited lateral vibration of the two cantilevered, telescoping tubes forming the joint. The joint design featured a localized annular constriction. Flowrate, modal damping, tube engagement length, and eccentric positioning were among the parameters tested. Interestingly, all self-excited vibrations could be avoided by following a simple design rule: place constrictions only at the downstream end of the annular region between the tubes. Also, overall modal damping decreased with increased flowrate, at least initially, for upstream constrictions while the damping increased for downstream constrictions.

I. INTRODUCTION

Main coolant flow paths through the components of a reactor system often parallel each other from one relatively stagnant plenum region to another. However, the flow paths and plenum regions are rarely completely sealed from each other because of other design requirements to allow for thermal expansion of components or their removal. Thus, leakage flow across pressure boundaries is not uncommon. When component vibration can interact and alter the leakage flow, the conditions for self-excited vibrations are present. Many reactor component designs have suffered from leakage flow-induced vibrations [1-3].

A review of leakage flow excitation mechanisms [2] has shown that self-excited vibrations can occur for each of the geometries in Fig. 1, regardless of whether the central component is interpreted as a plate (two-dimensional flow) or a cylinder (three-dimensional flow). The upstream constriction on the central tube in Fig. 1a can cause dynamic instability in a pure translational (vertical) vibrational mode because of the differences in local flow valving on opposite sides of the tube. According to available information, the constriction must block a significant portion of the flow channel before the mechanism is active, and when the constriction is moved to the downstream end of the leakage flow path, no instability occurs in a translational mode.

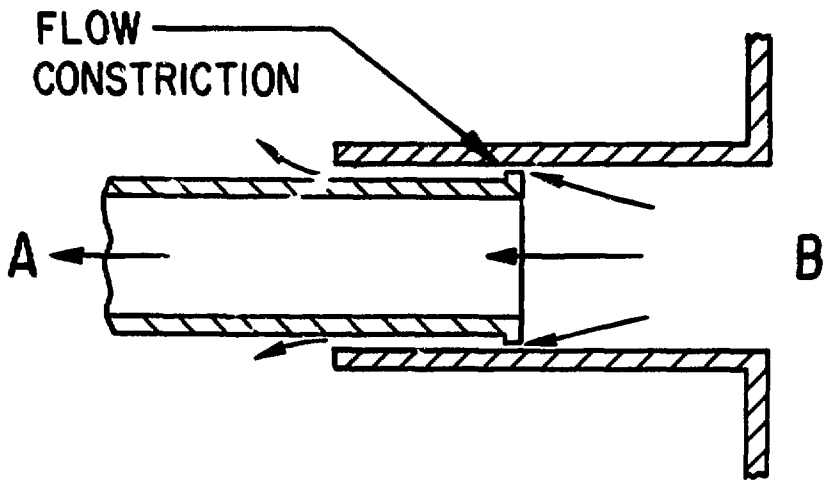

(a)

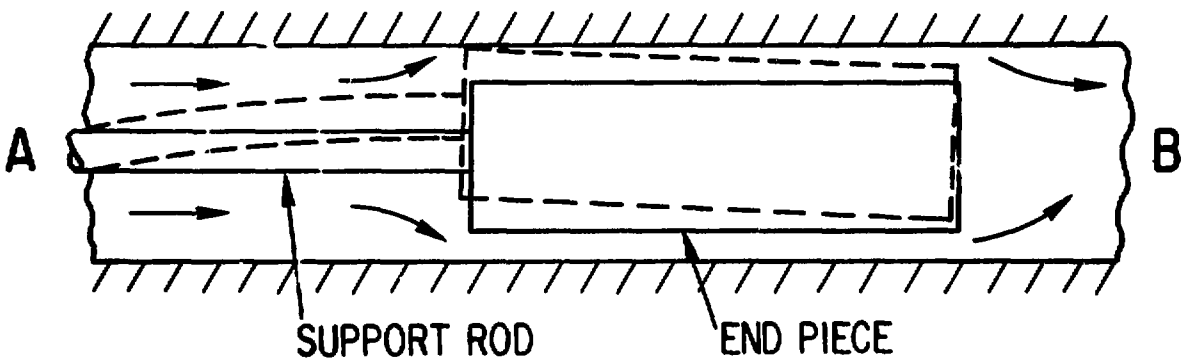

(b)

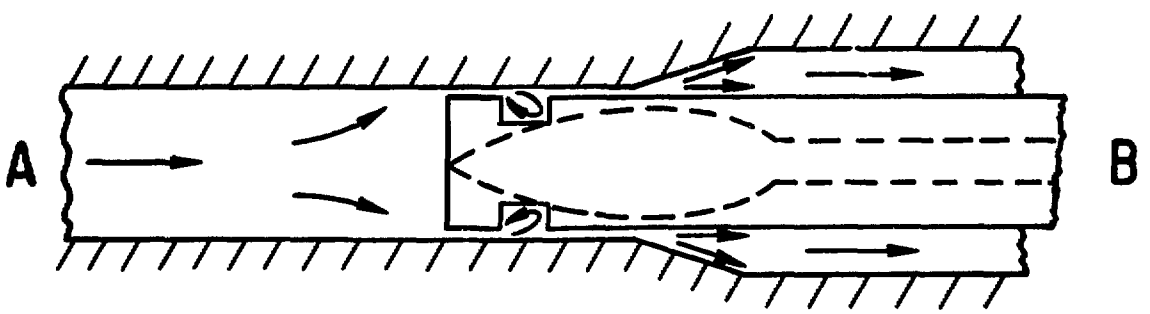

(c)

Fig. 1. Leakage Flow Geometries

If a central body can be excited into a rotational vibration motion, such as shown in Fig. 1b, then the local valving created may be associated with a dynamic vibration instability. Limiting the motion to a pure (vertical) translation and adding a downstream constriction have a tendency to statically force the central body to diverge to an equilibrium position closer to, or in contact with, the outer body.

The instability mechanisms cited above have their origin in adverse pressure distributions caused by local variations in the acceleration of the flow along the entire lengths of the central bodies. Because local flow acceleration depends on the rate at which the leakage flow gap opens and closes, fluid forces can be created in phase with the central body motion. When these in-phase forces (negative fluid damping) are dominant, a dynamic instability will occur.

Another mechanism that can create negative fluid damping is associated with a diverging leakage flow path, such as shown in Fig. 1c. Essentially, if the flow efficiency of the diverging (diffuser) section increases as the central body motion increases the throat size, then a dynamic instability is possible. Flow separation in the diverging (diffuser) section--out of phase with the displacement of the central body, and, therefore, possibly in phase with the velocity--was a specific mechanism identified with diffuser efficiency variations.

The mechanisms identifed and researched to date have been for relatively simple structural motions: the vibration (translation or rotation) of a single-degree-of-freedom rigid body ideally positioned in a rigid, stationary flow channel. All the analytical and experimental evidence that is available, which is not a lot, indicates that local geometry, more complicated vibration modes, and geometric eccentricities can greatly influence the existence of known instability mechanisms and/or create new ones. This may be the reason why the ability to analytically predict experimental results has been poor in almost every case.

Full-scale model testing of the more complicated slip joint geometry and structural motion of the CRBR upper and lower shroud tubes showed [4] that a translational leakage flow excitation mechanism did occur in the first vibration mode of the two telescoping, cantilevered tubes if the prototypic flow direction shown in Fig. 2 was reversed. Also, a second mode (rotational) excitation mechanism was thought to exist at higher flowrates just beyond the test facility pumping capacity. Any of the three excitation mechanisms discussed above could have been responsible for the unstable motion observed. Because of the inability to quantitatively predict instability flowrates, scale model testing will continue to be necessary for each new slip joint design.

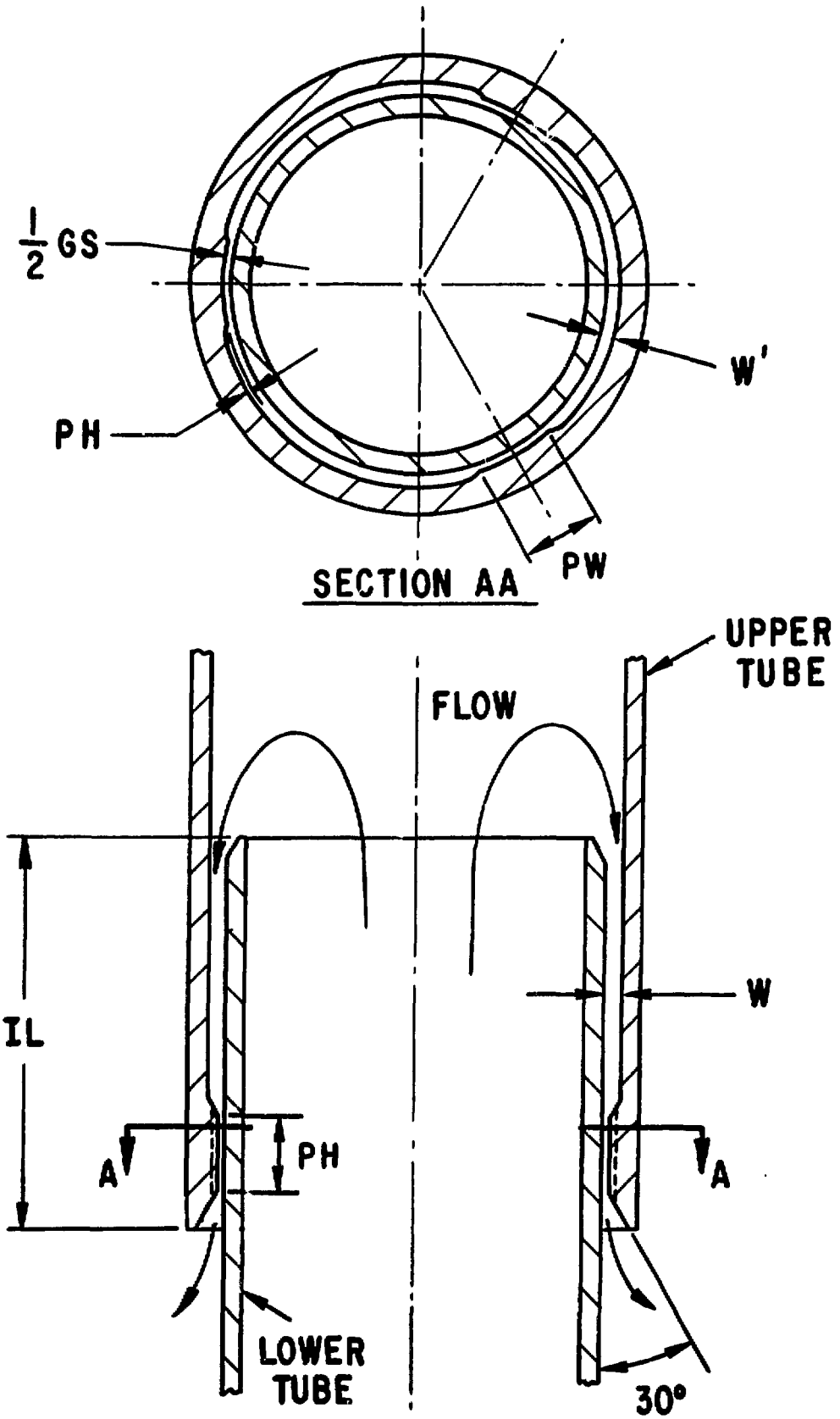

Fig. 2. CRBR Shroud Tubes Slip Joint

The expense of model testing and of repairing operating reactors can be reduced if reactor component supports that create leakage flow paths are limited to a few designs shown by comprehensive experimental and analytical research to be free of flow-induced vibration excitation mechanisms. With this goal in mind, comprehensive testing of a specific slip joint design, as in Fig. 2 with PH = PW = 0, for two telescoping tubes--one flexible and one rigid--was performed to define an operating parameter stability map indicating conditions for which no self-excited motion occurred. Although initially concentric tubes were used in the comprehensive testing reported here, preliminary testing indicates the same design can be used with initially eccentric tubes.

II. TEST FACILITY

To provide a means to extensively investigate the slip joint design, a leakage flow-induced vibration test facility was designed and constructed; where possible, parts were salvaged from the test of the CRBR shroud tubes [4]. In the new facility, parameter variation capabilities were enhanced: higher flowrates, reversible flow directions, variable damping in the fundamental mode, changeable local slip joint geometries, variable engagement length, and monitored displacements at the slip joint and the second mode antinode.

The main vessel of the facility was mounted in a pit, as shown in Fig. 3. The main vessel is an 18 in. (460 mm) diameter Schedule 10 pipe, ~18 ft (5.5 m) long. The model of the CRBR upper tube [6.5 in. (165 mm) OD x 5.5 in. (140 mm) ID and ~16 ft (4.9 m) long] was retained as the flexible tube of the new facility, but was cantilevered upward from the bottom flange of the main vessel. A new endpiece (Part 4 in Fig. 4) for the flexible tube and a new, relatively rigid tube and endpiece (Parts 3, 5, and 2) were constructed to replace the original endpieces of the CRBR shroud tubes.

The piping external to the main vessel in Fig. 3 allowed the flow direction to be reversed. With Valves V1 and V2 open and V3 and V4 closed, flow is bypassed from the accumulator tank of a central flow facility to enter the top of the main vessel through the rigid upper tube. Then the flow passes through the slip joint into the main vessel plenum before exiting (just below floor level) through the outlet to the open tank of the Flow-induced Vibration Test Facility (FIVTF). This is called upward flow because its direction is upward through the slip joint. By closing V1 and V2 while opening V3 and V4, the flow direction could be reversed (downward flow). In either case, control Valves CV1-CV3 and Flowmeters FM1-FM3 were used to throttle and measure the flow. Only a fraction (~10%) of the flow

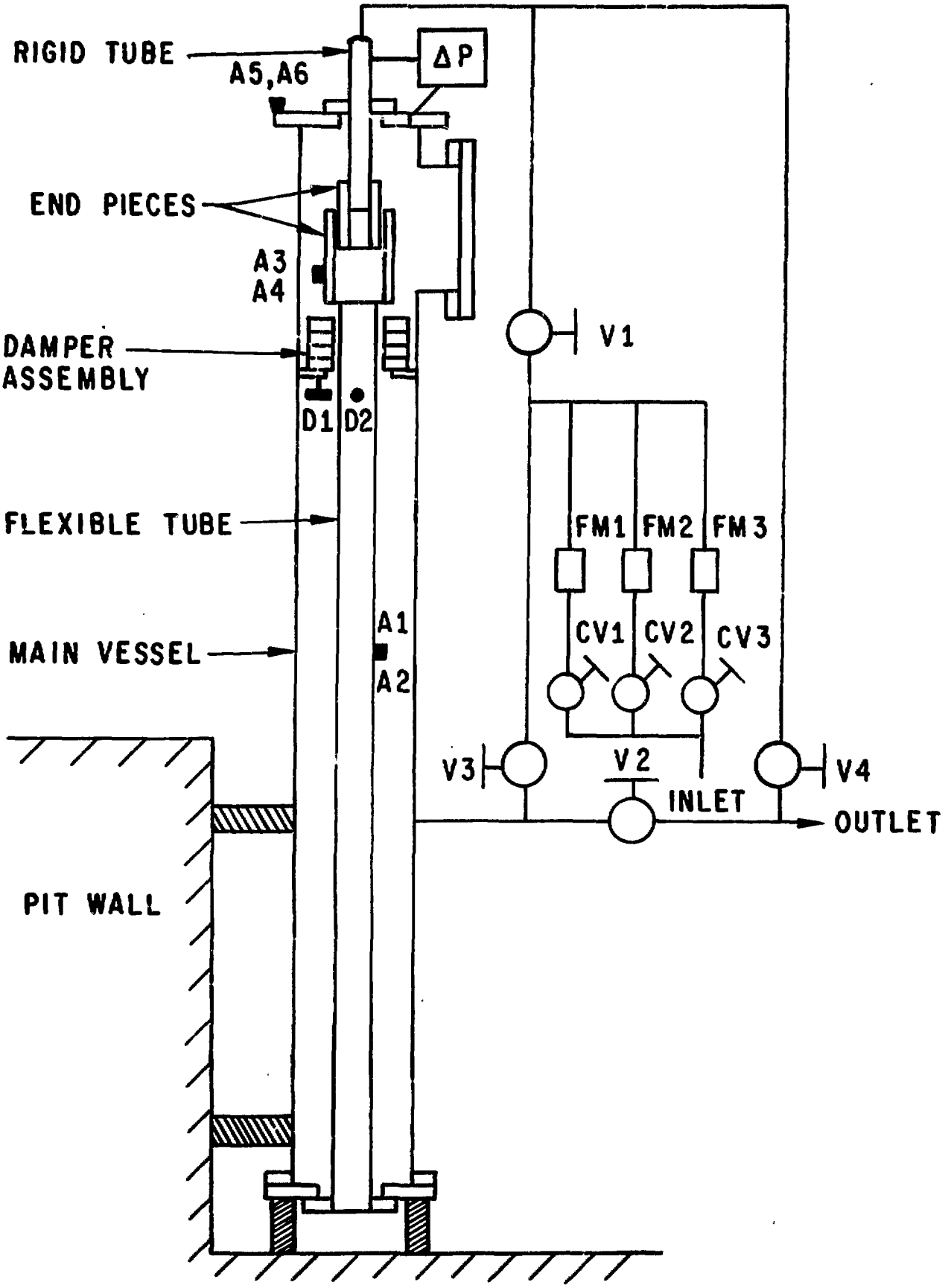

Fig. 3. Leakage Flow-induced Vibration Test Facility

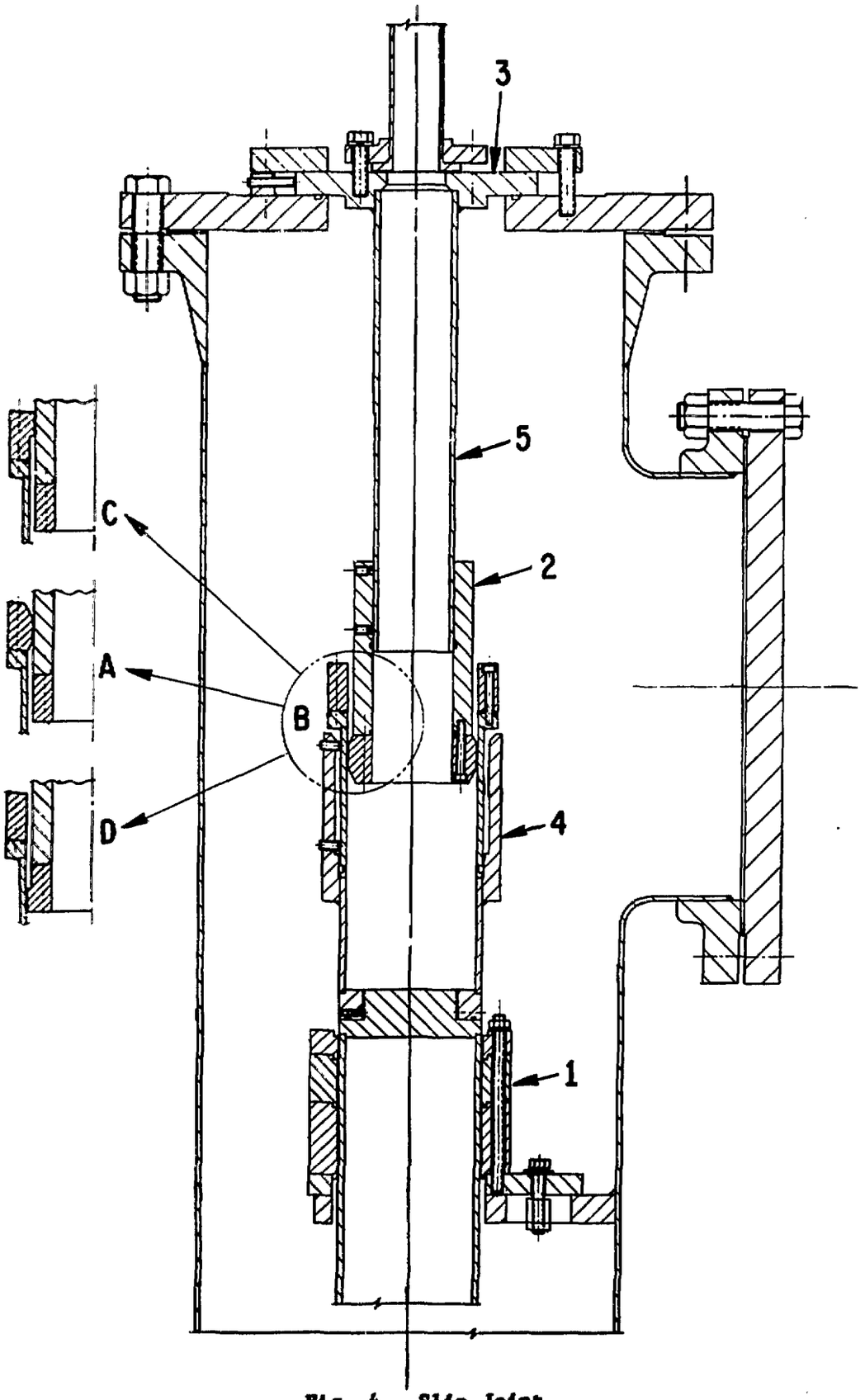

Fig. 4. Slip Joint

in a main leg of the FIVTF was bypassed to the inlet to the leakage flow facility to assure a constant inlet pressure.

In the new design, the constriction size W' (defined in Fig. 2) could be varied by changing the removable endpieces on either the flexible or rigid tube (Cases A-D in Fig. 4). The engagement length IL could be varied by sliding the endpiece (Part 2) to different axial positions along the rigid tube (Part 5). The flow direction in the slip joint could be reversed by external valving, as discussed above, or by changing endpieces on both tubes while maintaining the same direction of flow through the external piping. The annular gap size W between the tubes could be changed by slipping sleeves over the endpiece on the rigid tube (Part 2) or in the endpiece on the flexible tube (Part 4).

Modal damping could be changed by stacking different numbers of rings in the squeeze film damper assembly (Part 1). The squeeze film damper assembly, which was designed based on available information [5], was expected to allow variation of the modal damping from ~1-8% of critical damping in the fundamental mode. For the same damper assembly configurations, very little change in damping was predicted for the primarily rotational second mode. The shape of the constriction could be changed and the simultaneous existence of both upstream and downstream constrictions could be achieved by replacement of the slip joint endpieces (Cases A-D in Fig. 4). Eccentric location of the rigid and flexible tube could be achieved by moving the entire rigid tube assembly (Parts 2 and 5) with respect to the upper (top) flange of the main vessel (Part 3). Positioning thumbscrews were provided in two orthogonal directions to effect the small eccentric movements of the plate on which the rigid tube is mounted.

III. TEST DEFINITION

Not all parameter variations possible with the new facility were used in the testing reported here--only slip joint A of Fig. 4 has been tested. In Design A, a raised diameter of D = 5.5 in. (139.7 mm) on the flexible tube (air fundamental frequency, f_1 ~4.1 Hz) forms a 1 in. (25.4 mm) long by W' = 0.040 in. (1.0 mm) wide annular gap with the rigid tube (fundamental frequency >75 Hz). The entrance and exit to this primary annular region is beveled at 30°, with respect to the vertical, until a secondary W = 0.28-in. (7.1-mm) wide annular region is formed between the tubes. The test matrix included varying the flowrate through the slip joint from ~1.5 gpm (9.5×10^{-5} m^3/s) to 110 gpm (6.94×10^{-3} m^3/s), the first mode damping as a percentage of critical damping from ζ_1 = ~0.5 to 6.5%, and the engagement length of the two telescoping tubes from L = 1.56 in. (39.6 mm) to 5.0 in. (127.0 mm). For L = 1.5 in. (38.1 mm), no secondary annular region exists

and the bottom of the primary region is even with the end of the rigid tube. The above test matrix was performed for initially concentric tubes. Also, one flow test was performed to indicate whether designs for concentric tubes on the borderline of instability remained so for the worst (almost touching) case of eccentric tubes.

The nominal radial gap between the raised diameter on the flexible tube and the inside diameter of the rigid tube was measured to be within 1% of the design specification. After alignment, the concentricity was measured and found to be maintained within 6.3% of the radial gap for all engagement lengths. The damper assembly was erected and the damper rings aligned concentrically, as well as possible, around the flexible tube. Because the flexible tube is pipe stock, the radial gap formed at the damper assembly varied with the number and location of the rings. However, variations in gap size were not as important as reproducing similar damping values for each test. Therefore, prior to any flow testing, combinations of rings were identified that gave the desired damping values. Appropriate combinations of rings were reproduced for flow testing and prior to each test damping measurements were made.

IV. INSTRUMENTATION

Since motion of the flexible cantilevered tube as a function of pressure drop and flowrate was of prime interest for each slip joint geometry and value of initial modal damping, the absolute displacement of the end of the flexible tube was measured in two orthogonal directions with the displacement gauges D1 and D2 (see Table 1) located on the damper assembly support plate (as shown in Fig. 3). Accelerometers A1-A4 were included to measure relative motion in the second mode of vibration where a node exists near the slip joint and an antinode near Accelerometers A1 and A2. Accelerometers A5 and A6 were used initially to assure there was no coupling between the flexible tube and the main vessel in the frequency range of interest. The static pressure drop ΔP across the slip joint leakage flow path was measured with differential pressure gauges P1 or P2 and the flowrates were measured with three 1 in. (25.4 mm) turbine flowmeters, F1-F3.

Displacement gauges D1 and D2 were waterproofed to 100 psi in water and calibrated with a micrometer (Kaman model 830854-001) accurate to 0.1×10^{-3} in. (2.54×10^{-3} mm). Since the gauges were mounted ~20.5 in. (0.52 m) below the top of the flexible tube endpiece, the displacement gauges read only ~85% of the motion at the constriction because of the variation in mode shape with distance along the flexible tube. Displacement gauge D1

Table 1. Instrumentation Used in Slip Joint Test

No.	Transducer	Location	Amplifier	Sensitivity
A1	Accelerometer, Endevco Model 2220C	E-W, top	Endevco Charge Amplifier Model 2735	0.1 g/V
A2	Accelerometer, Endevco Model 2220C	E-W, antinode	Endevco Charge Amplifier Model 2735	0.1 g/V
A3	Accelerometer, Endevco Model 2220C	N-S, top	Endevco Charge Amplifier Model 2735	0.1 g/V
A4	Accelerometer, Endevco Model 2220C	N-S, antinode	Endevco Charge Amplifier Model 2735	0.1 g/V
D2	Displacement Gauge, Kaman Model KD 1100-2S	N-S	Kaman Oscillator Demodulator Model 2300-2S; Kaman Power Supply, Model P3100	0.1 in./V
D1	Displacement Gauge, Kaman Model KD-1100-2S	E-W	Kaman Oscillator Demodulator Model 2300-2S; Kaman Power Supply, Model P3100	0.1 in./V
P1	Pressure Gauge, Viatran Model 209 (50 psi maximum)	Rigid Tube	Unholtz-Dickie Bridge Conditioner Model D22PMB	10 psi/V
P2	Model 209 (10 psi maximum)	Below Joint	Unholtz-Dickie Bridge Conditioner Model D22PMB	1 psi/V
FM1	Flowmeter, Brooks Model 4901-16		Pulse Self-Generator	0.06250 gpm/Hz
FM2	Flowmeter, Brooks Model 4901-16		Pulse Self-Generator	0.06250 gpm/Hz
FM3	Flowmeter, Brooks Model 4901-16		Pulse Self-Generator	0.06150 gpm/Hz
F1	Force Transducer, PCB 208A02		PCB 464A, ICP Amplifier	5.0 lb/V

monitored motion in the east-west (E-W) direction while D2 monitored in the north-south (N-S) direction.

The four accelerometers were mounted in two watertight (100 psi) capsules such that two orthogonal directions of motion could be monitored by each capsule. Before the capsules were attached to the flexible tube, they were mounted on a small shaker and their sensitivities were adjusted to produce nominally the same acceleration at 20 Hz for displacements up to 0.040 in. (1.0 mm) peak to peak. Then one capsule was mounted 5 in. (127 mm) below the top on the north side of the flexible tube and the other 105 in. (2.67 m) from the top on the south side of the flexible tube. A1 (A3) at the top of the tube and A2 (A4) at the antinode of the second mode measured accelerations in the E-W (N-S) directions, respectively, but they were out of phase by 180°.

Static differential pressure transducers (P1 and P2) were calibrated using a pulse calibrator (PCB Model 903A02) readable to 0.2 psi. The pressure transducer (P1) was employed with an orifice flowmeter (Daniel Simplex Orifice Plate Holder H745W) to calibrate the three turbine flowmeters (FM1-FM3) already permanently installed in the flow facility. The two pressure gauges were installed to measure pressure drop between the plenum outside the slip joint and inside the flexible tube ~12 in. (304 mm) below the slip joint or inside the rigid tube the same distance above. During flow testing only the transducer above the joint was used after establishing that both locations produced essentially the same static pressure drop. The rigid tube pressure drop was subject to much smaller dynamic pressure fluctuations.

V. STRUCTURAL CHARACTERIZATION

Prior to any flow testing, the frequencies and structural damping of the first two modes of the flexible tube in air and nonflowing water were determined with the annular squeeze film damper assembly submerged but without any water in the slip joint. This preliminary testing not only provided baseline information for the dynamic behavior of the flexible tube, but also provided a means to select combinations of damping rings for flow testing. Structural damping in the fundamental mode was determined by measuring the motion of the flexible tube with the displacement gauges D1 or D2 while exciting the tube with known random excitation forces in the E-W direction or by pluck (transient decay) testing in the E-W and N-S directions.

The random forces were created between a bar magnet attached to the flexible tube and two electromagnetic solenoids attached to a common frame. The bar magnet, which was 0.625 in. (15.9 mm) in diameter and 3 in.

(76.2 mm) long and made of Alnico 8, was symmetrically located along the axis between the two solenoids in a fashion similar to the calibration setup shown in Fig. 5. The calibration setup was used to establish the current levels and gap sizes between the magnets and solenoids that would produce the desired force levels and displacements. Both the common frame and bar magnet shown in Fig. 5 are isolated from their support by force transducers. During damping measurements, the motion of the flexible tube was maintained at <10% of the gap between the magnet and the solenoid core bar to avoid amplitude dependent magnetic forces. A piezoelectric force gauge, identified as F1 in Table 1, isolated the common frame, on which the electromagnets were mounted, from the pressure vessel support and was used to measure forces. The piezoelectric force gauge was calibrated, almost to zero frequency, by measuring voltage output generated by lifting known weights, from 0.22 to 1.10 lb (0.98 to 4.89 N), off the transducer face mounted in a horizontal plane.

A low-pass (10 Hz) random-control voltage was generated using the digital-to-analog converter of a Hewlett Packard (HP) 5451C Fourier analyzer. The control voltage was input into a DC audio amplifier that provided current to solenoids. The random force generated in this fashion had the attribute of being periodic in the analysis time window of the analyzer, thus avoiding the leakage error that would occur for an ordinary random signal.

The HP 5451C Fourier analyzer was used to obtain transfer functions between the random excitation force and the motion as measured by the displacement gauges in the E-W direction. The natural frequencies and modal damping were measured directly from the transfer function plots by the half-power point method or from curve fits generated by the modal analysis software of the HP 5451C analyzer. Also, pluck testing and motion decay measurements (log decrement) were performed in the E-W and N-S directions using both the displacement gauges and accelerometers. Both types of testing were performed at different amplitude levels in air and water.

Structural testing in air determined the first two modal frequencies to be 4.1 and 29 Hz. N-S was the preferred direction of motion for free vibration in the fundamental mode. Motion initiated in the N-S direction would result in a linear orbit that decayed with time. Motion initiated in the E-W direction would quickly lead to an elliptical orbit with major axes in the N-S direction. This directional preference in the fundamental mode was reflected in the percent of critical damping measurements, which ranged from 0.05-0.11% in the N-S direction to 0.19-0.33% in the E-W direction. The second mode was so very lightly damped (0.026-0.034%) that measurement was difficult.

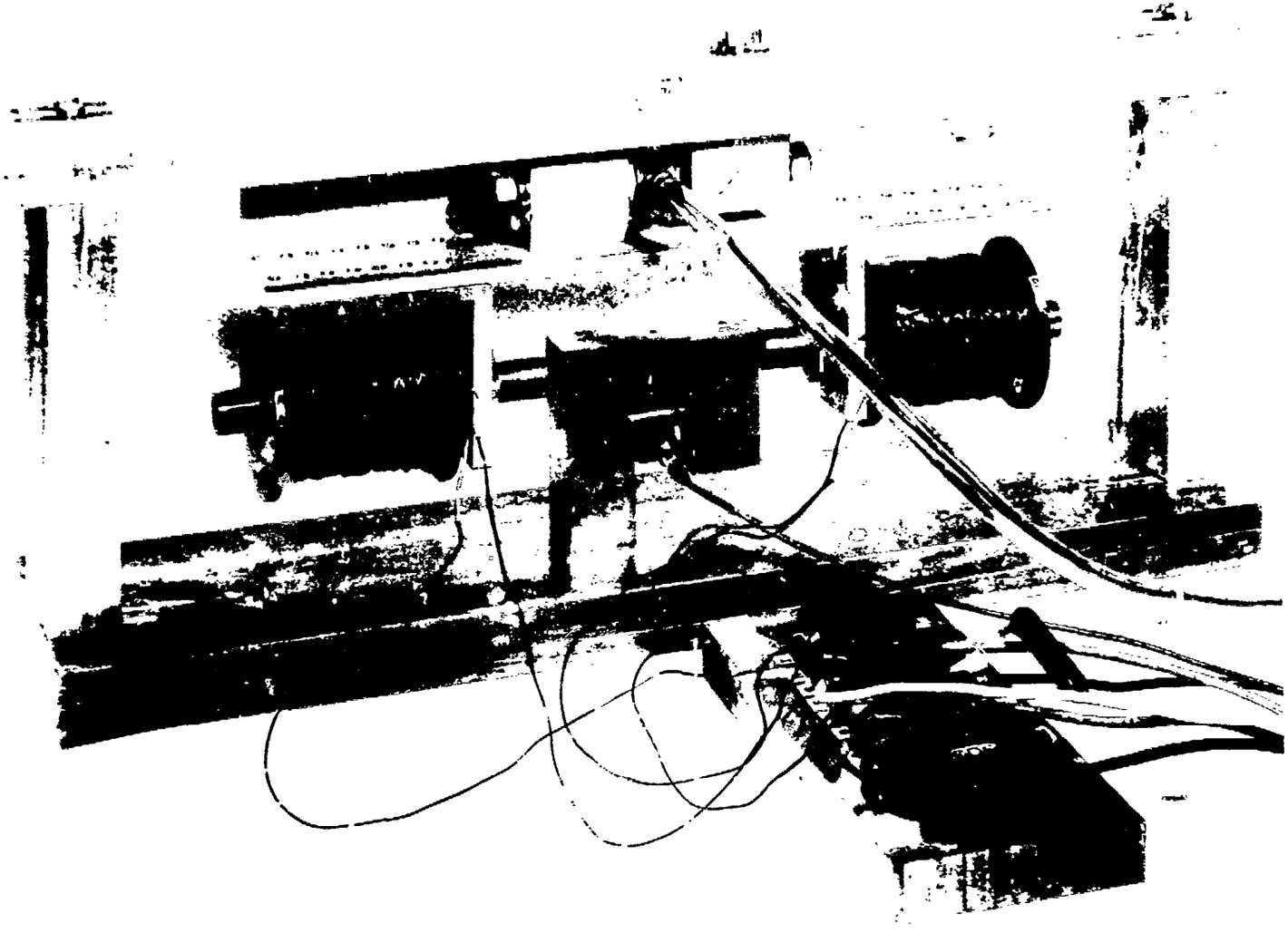

Fig. 5. Electromagnetic Exciters and Intervening Bar Magnet in Calibration Fixture. ANL Neg. No. 113-78-561

Structural testing in water without the damping rings or a rigid tube found natural frequencies of 3.5 and 22 Hz, with damping in the fundamental mode of 0.17-0.26% in the N-S direction and 0.73-1.1% in the E-W direction. The damping in the second mode was ~0.13%. The directional preference in the first mode remained.

Six combinations of damping rings were tested by random and plucking excitation. Damping in the E-W direction was difficult to measure for small amplitudes [<0.001 in. (0.025 mm) RMS] of random excitation or when the end cycles of a pluck test were of similarly small amplitude. These results were not used. Some increases in damping for increased vibration amplitudes were observed in range [0.001-0.005 in. (0.025-0.13 mm) RMS], but most were within the accuracy of the measurement method. The average values of the fundamental frequency and structural damping are given in Table 2 along with predictions [5]. The predictions are conservative, but give a reasonable estimate of damping (within 30%) and a method of designing the damping rings.

Table 2. Fundamental Frequencies and Structural Damping without Slip Joint Submerged

Damping Ring Depth (in.)	Measured Frequency (Hz)	% Critical Damping		
		E-W	N-S	Predicted
air	4.1	0.2	0.1	0.1
0	3.5	0.4	0.2	0.2
1	3.5	0.6	0.5	0.6
2	3.4	1.3	1.1	1.5
3	3.3	2.0	2.2	3.2
4	3.1	3.4	3.3	4.8
5	2.9	5.1	4.9	6.1
6	2.8	6.9	6.6	7.5

During flow testing, the percentage of critical damping in the first mode ζ_1 was measured, including the case of no flow with the slip joint submerged, by plucking the flexible tube in the N-S direction with initial peak amplitudes of 0.0025 in. (0.064 mm) to 0.006 in. (0.15 mm). Pluck testing in the N-S direction in this amplitude range was expected to give the most repeatable results, based on the previous damping measurements. In particular, excitation at higher amplitudes would have resulted in higher damping (nonlinear, large motion effects) and excitation in the E-W direction would have produced much less repeatable, highly orbitable motion

because the preferred direction of motion was in the N-S direction. The electromagnetic coils used to produce random excitation could be used only in the E-W direction, so only N-S pluck testing was employed during flow testing.

For no flow, the first-mode frequency f_1 and ζ_1 for submerged damping rings and slip joint depended on the height H of the damping rings and, as can be seen in Table 3, only slightly on the length of engagement L. As a result, changes in ζ_1 or L should affect instabilities independently. Note that L/D = 0 and H/D = 0.0 in Table 3 correspond to an unsubmerged slip joint and damping rings, respectively. Means were not available to alter the damping in the second mode, which was ζ_2 ~0.3% at f_2 ~21 Hz for all cases, but the qualitative effects on instabilities are expected to be similar to those observed for damping changes in the first mode.

VI. INSTABILITY CONDITIONS

For a flow direction from the top to the bottom of the slip joint, self-excited motion occurred for many flowrates, engagement lengths, and structural damping values. However, values for each parameter were identified for which self-excitation did not occur. For a flow direction from the bottom to the top of the slip joint, no self-excited motion was observed in any modes for any of the flow parameters tested.

Top to bottom flowrates, the L, and the ζ_1 for which instabilities were observed are given in Fig. 6. The open symbols, solid symbols, and solid line indicate first-mode instabilities, second-mode instabilities, and bounds on regions of parameter values below which neither a first nor a second mode instability occurred. The general trend was that instabilities were more likely for longer engagement lengths and smaller structural damping values. However, threshold values for both parameters appeared to exist. Most importantly, instabilities were not observed for engagement lengths less than 2.25 in. (57.2 mm).

If a first-mode instability occurred for a given engagement length and damping, then motion at the slip joint usually increased with flowrate until impacting of the tubes occurred with mixed modes of vibration. The exception was for L = 3.0 in. (76.2 mm), where first-mode unstable motion occurred in a limit cycle with small amplitude over only a small range of flowrates. When a second-mode instability occurred without a prior first-mode instability, impacting did not necesarily occur at higher flowrates because the slip joint was very near the node of the second mode. In Fig. 6, a slash through a symbol means unstable motion ceased at this flowrate, but sometimes the instability would reappear at a higher flowrate. Cessation of unstable motion was associated with the second mode, except in

Table 3. First-mode Frequency f_1 (Hz) and Structural Damping ζ_1 (%) for Different Engagement Lengths (L), Damping Ring Heights (H), and No Flow

H/D	L/D					
	0.0	0.28	0.46	0.55	0.64	0.91
0.0	4.1, 0.1	4.1, 0.1	4.1, 0.1	4.1, 0.1	4.1, 0.1	4.1, 0.1
0.18	3.5, 0.5	3.1, 0.6	3.1, 0.6	3.1, 0.6	3.0, 0.75	3.0, 0.9
0.55	3.3, 2.2	2.9, 1.6	2.9, 1.6	2.9, 1.7	2.9, 1.75	2.85, 1.9
0.73	3.1, 3.3	---, ---	2.8, 2.5	2.8, 2.8	2.8, 2.8	2.75, 2.85
1.09	2.8, 6.6	2.55, 6.0	---, ---	2.5, 5.9	2.5, 6.0	2.5, 5.8

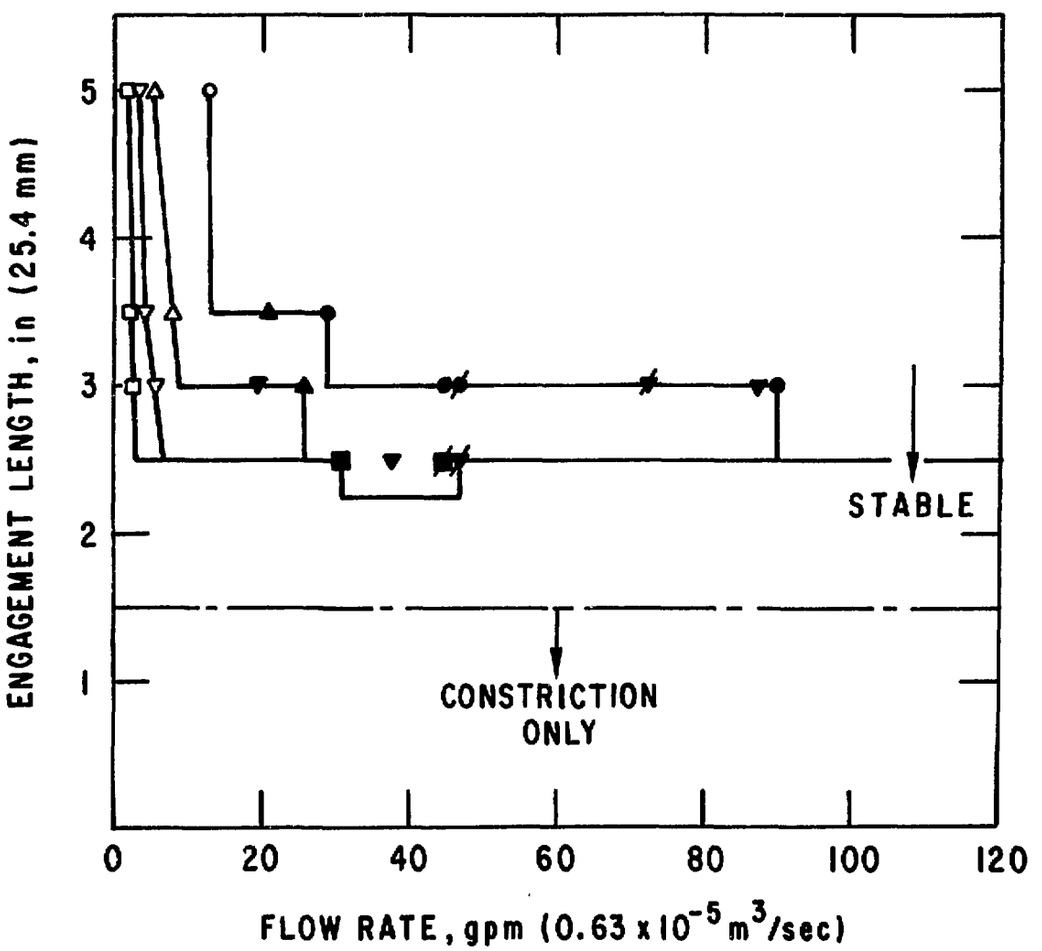

Fig. 6. Instability Map for Top-to-Bottom Flow where First Mode ζ_1 (%) = 0.5, □; 2.2, ▽; 3.3, △; 6.6 ○ (The solid symbols indicate instability in the second mode: $f_2 \cong 21$ Hz, $\zeta_2 = 0.3$. The solid line (——) bounds stable regions.)

the one case [L = 3.0 in. (76.2 mm)]. However, in many cases, a first-mode instability was dominated by a second-mode instability at higher flowrates.

Flow damping measurements showed, as discussed below, that the large motion in the first mode was a true self-excited instability. Flow damping measurements were not made for the second mode, so it is possible that motion in the second mode was forced and not a self-excited instability. Indicators of a true second-mode instability were that the motion always occurred at the second-mode natural frequency, large-amplitude perturbations often had to be created to initiate the motion, and second-mode motion existed for all flowrates above a threshold value for many parameter values.

No unstable motion was observed for bottom-to-top flow through slip joint A in Fig. 4. During CRBR acceptance testing for the flexible shroud tube [4], unstable motion appeared to be imminent at the highest flowrate, Q ~50 gpm (3.15^{-4} x 10 m^3/s). However, testing in the leakage flow facility showed only relatively large forced random motion in the second mode at and above this flowrate.

For those cases in which instabilities did not occur, the flexible tube did not remain concentric with respect to the rigid tube. Usually the flexible tube would diverge statically, with the amplitude increasing monotonically with flowrate. The direction of divergence was not unique and probably was biased by the slight variations from exact concentricity that always were present due to thermal expansion effects. The size of the static divergence varied from 10 to 50% of the gap, but the two tubes never contacted unless an instability occurred. Superimposed on the static deflection of the flexible tube were dynamic fluctuations, but they never exceeded ~18% of the gap. The greatest dynamic fluctuations occurred for the case of smallest damping and engagement length. This was the case where the fluctuations were mistaken as an incipient second-mode instability during CRBR acceptance testing. Static divergence would occur in unstable cases below the critical flowrates, but the direction was erratic and the magnitude did not vary monotonically with flowrate. This was especially true for cases where second- but not first-mode instabilities existed.

VII. FLOW DAMPING

The flexible tube's total damping for first-mode motion in the N-S direction is shown in Figs. 7-9 for different values of structural damping (H/D), different engagement lengths (L/D), and different flowrates for top-to-bottom flow. As noted above, self-excitation occurred only in the top-to-bottom flow direction through the slip joint. The cases for which self-excitation occurred can be recognized by damping curves that decrease with increasing flowrate and ultimately go to zero at some critical

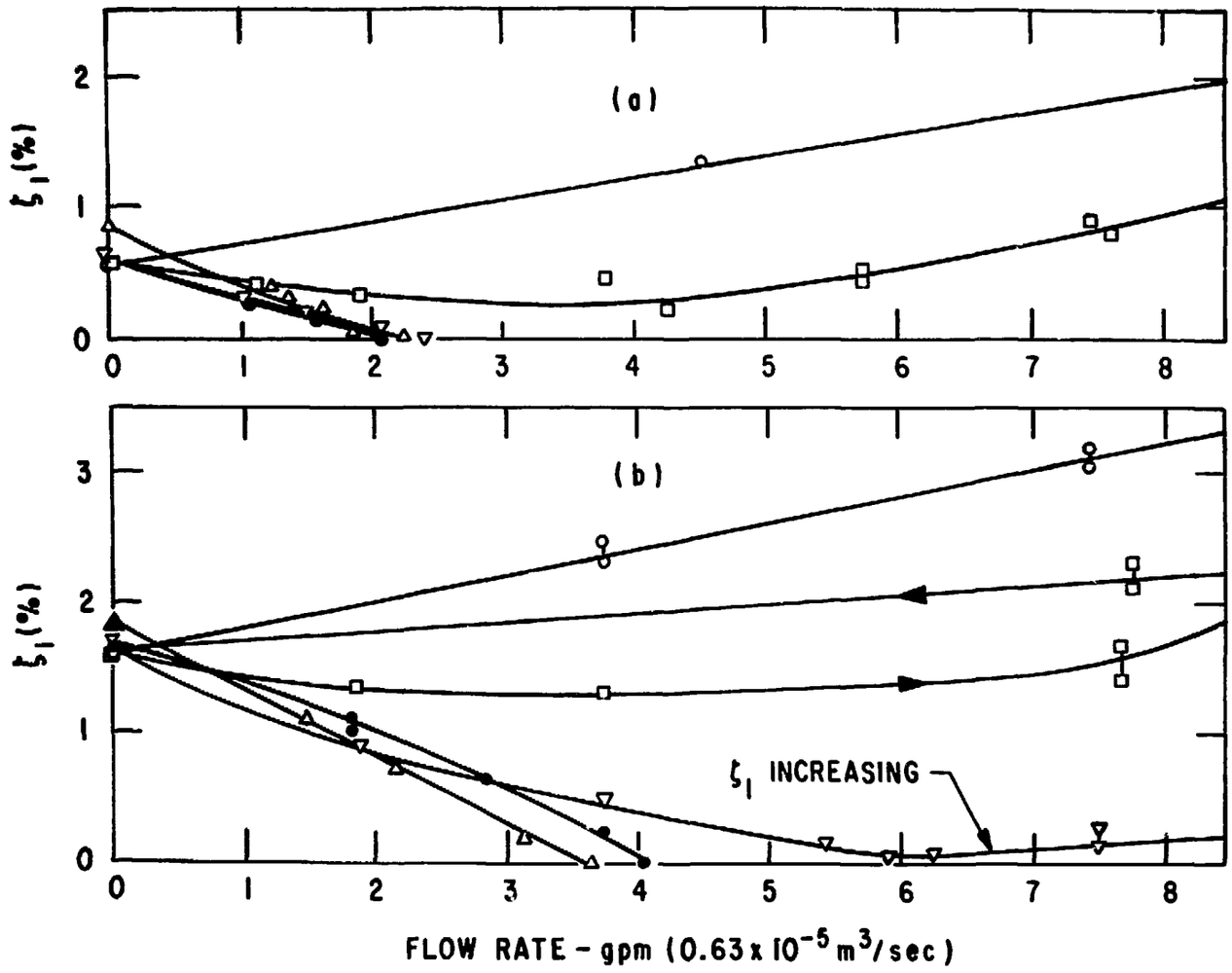

Fig. 7. Variation in First-mode Damping with Top-to-Bottom Flow for (a) H/D = 0.18 and (b) H/D = 0.55 where L/D = 0.28, ○ ; 0.46, □ ;0.55, ▽ ; 0.64, ● ; 0.91, △

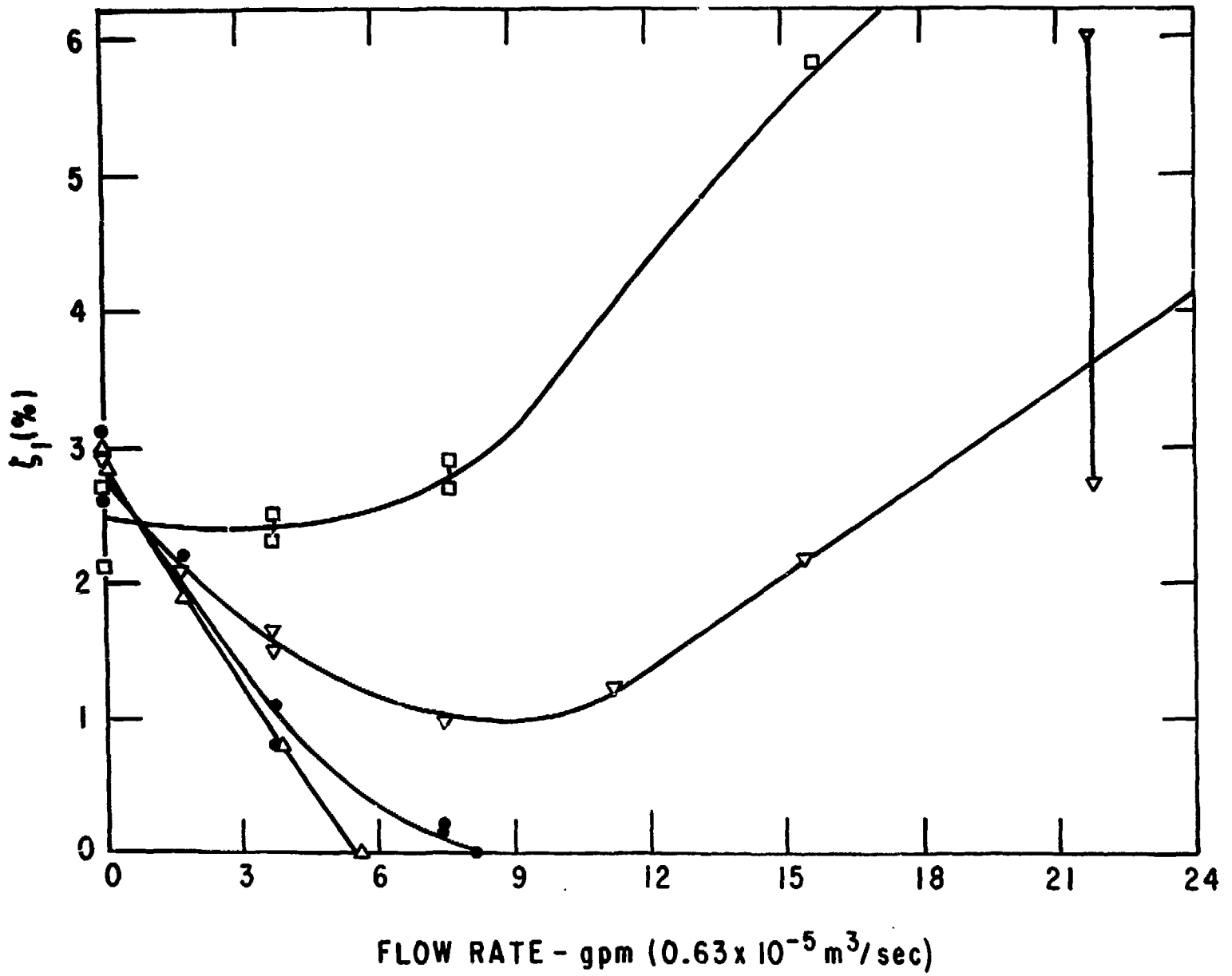

Fig. 8. Variation in First-mode Damping with Top-to-Bottom Flow for H/D = 0.73 and L/D = 0.28, ○; 0.46, □; 0.55, ▽; 0.64, ●; 0.91, △

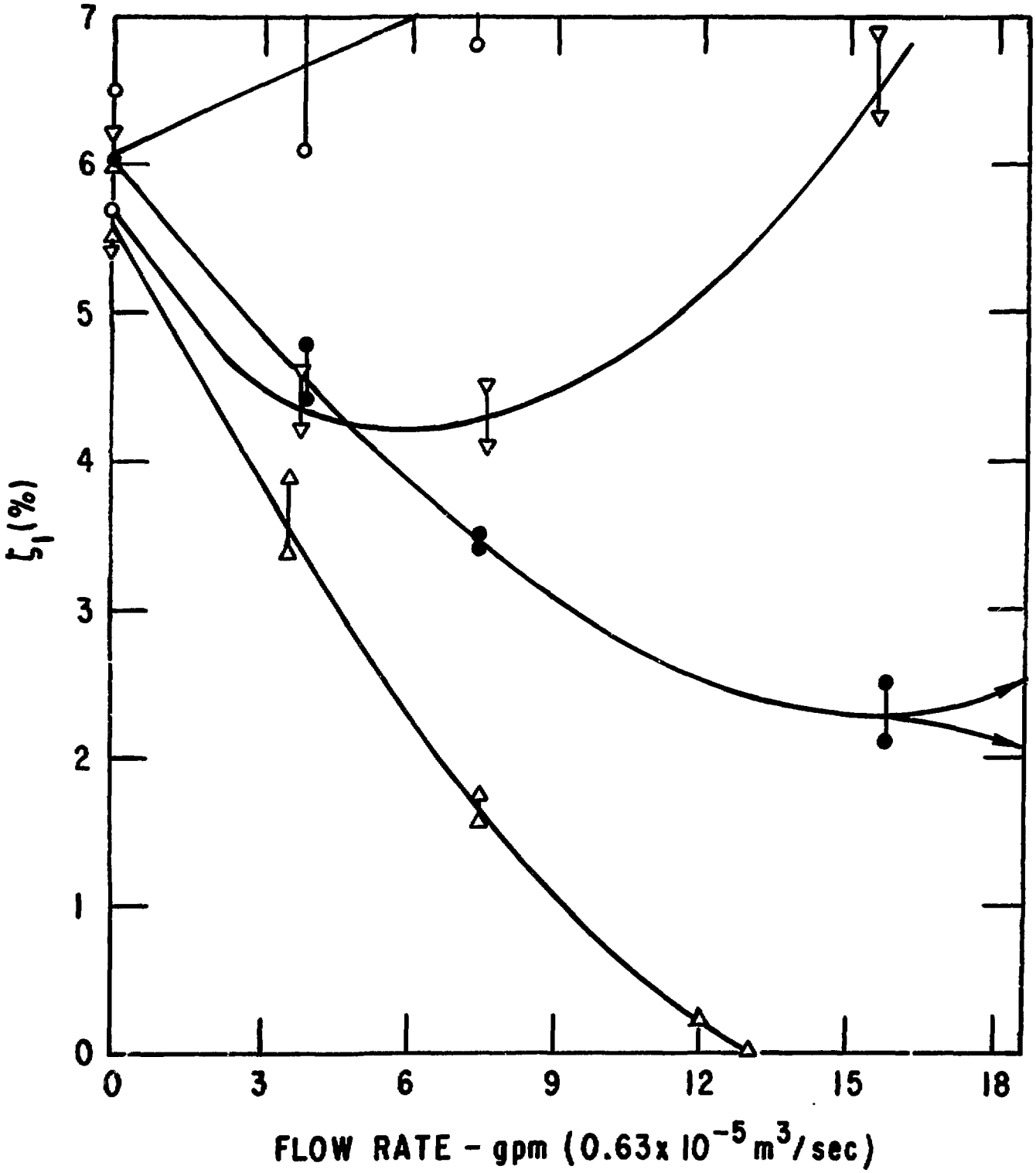

Fig. 9. Variation in First-mode Damping with Top-to-Bottom Flow for H/D = 1.09 and L/D = 0.28, ○; 0.46, □ ; 0.55, ▽ ; 0.64, ● ; 0.91, △

flowrate. The first-mode data for the stability map in Fig. 6 were generated by plotting these critical flowrates.

Not all the cases where damping begins to decrease with an increase from zero flow result in self-excited motion. As can be seen for H/D = 0.18 or 0.55 and L/D = 0.46, H/D = 0.73 and L/D = 0.46 or 0.55, and H/D = 1.09 and L/D = 0.55 or 0.64, the damping decreases to a minimum that is not zero and then increases with increasing flowrate. In essence, for a given engagement length, threshold values of structural damping exist above which self-excited motion does not occur. In one case, H/D = L/D = 0.55, the structural damping was right at a threshold value. The total damping went to zero at a flowrate of ~6 gpm (3.78×10^{-5} m^3/s) and self-excited motion was initiated, resulting in a very well defined cycle of motion but with a very small amplitude. With increased flowrate, the self-excited motion ceased, as indicated by the increasing damping.

All the self-excited motion, at least near the critical flowrates, resulted in orbital motion with well defined frequencies and limited amplitude. In this case, limited amplitude motion means the amplitude did not increase without bound but remained finite for a given flowrate. Also, if the flexible tube was forced to a larger amplitude motion, a transient period of decay motion to the limit cycle occurred. If the flexible tube was held from moving and released, a transient buildup of motion to the limit cycle occurred. The orbitable motion was repeated but over long time periods. Most often, irregular precession occurred with increasing and decreasing orbit amplitudes. This behavior is believed to be due, in large part, to the nonlinear increases that occur in damping for increased amplitude motion in fluid-filled annuli [5], and the anisotropic structural damping properties of the flexible tube: there is greater structural damping in the E-W direction than in the N-S. Depending on H/D and L/D, increases in flowrate beyond the critical flowrates led, except for H/D = L/D = 0.55, to larger-amplitude limit cycle motion that resulted in impacting with the rigid tube or transition to dominantly second-mode motion.

Often large-amplitude motion occurred in the second mode but not in the first mode (see, for example, L = 2.5 in. (63.5 mm) and L = 3.0 in. (76.2 mm) in Fig. 6). Some indication of incipient motion in the second mode could be discerned in first-mode damping measurements. In particular, repeatability of measurements became difficult, as illustrated by the wide spread in data values for H/D = 0.73 and L/D = 0.55 in Fig. 8 or H/D = 1.09 and L/D = 0.64 in Fig. 9. In one case, H/D = 0.55 and L/D = 0.46 in Fig. 7, the damping values resulted in considerably different values before and after a second-mode instability occurred. The arrows in Fig. 7 indicate increasing and decreasing flowrates.

No self-excited or periodic random motion was observed for the bottom-to-top flow direction--only random motion, which increased in amplitude as the flow increased. As would be expected, the flow damping increased with increased flowrate, as the examples of Fig. 10 show for the extremes in structural damping. However, the rate of increase depended on the length of engagement. Interestingly, the longer the engagement the larger the flow damping for a given flowrate. Thus a larger engagement length is beneficial in stabilizing vibratory motion for bottom-to-top flow but detrimental for flow in the opposite direction. The scatter in the data shown in Fig. 10 does not indicate second-mode incipient motion, but the difficulty in measuring large values of damping by transient decay testing.

VIII. FLOW EFFECTS ON MODAL FREQUENCIES

The fundamental frequency of the flexible tube increased significantly with increased rates of flow, indicating that flow through the slip joint laterally stiffens the structure in addition to modifying total modal damping. This effect is best seen in Figs. 11b and 12b for bottom-to-top flow, because no other instabilities or hardening effects, such as impacting with the rigid tube, were present. Only data for the smallest and largest structural damping are shown. For top-to-bottom flow the trends are more confused (see Figs. 11a and 12a) because of unstable motion in the first two modes. The exception was the smallest engagement length, $L/D = 0.28$, for which no instabilities occurred in either flow direction. As can be seen by comparing the solid lines drawn through the $L/D = 0.28$ data points in Figs. 11 and 12, the trend of increased frequency with increased flowrate is the same for both flow directions, but the magnitudes of the trends were not the same. Bottom to top flow always resulted in higher frequencies, although at lower flowrates the differences with top-to-bottom flow were small. When a first-mode instability occurred, much greater hardening was observed, as illustrated by the $L/D = 0.91$ data in Fig. 11a, where impacting occurred at the highest flowrates. When second-mode excitation was present or incipient, the variations in the value of fundamental frequency were large, as illustrated by data for $L/D = 0.46$ in Fig. 11a and $L/D = 0.55$ in Fig. 12a.

Increases in the frequency of the second mode for increased flowrates were small for both stable and unstable motion in either mode (see Figs. 11 and 12). This result might be expected, since the node of the second mode occurs close to the slip joint. The data imply that flow through the slip joint is not an effective source of rotational stiffness. The only other trend is that the second-mode frequency is slightly smaller when a first-mode instability is present or incipient, as illustrated by the data for $L/D = 0.28$ versus $L/D = 0.91$ in Fig. 11a.

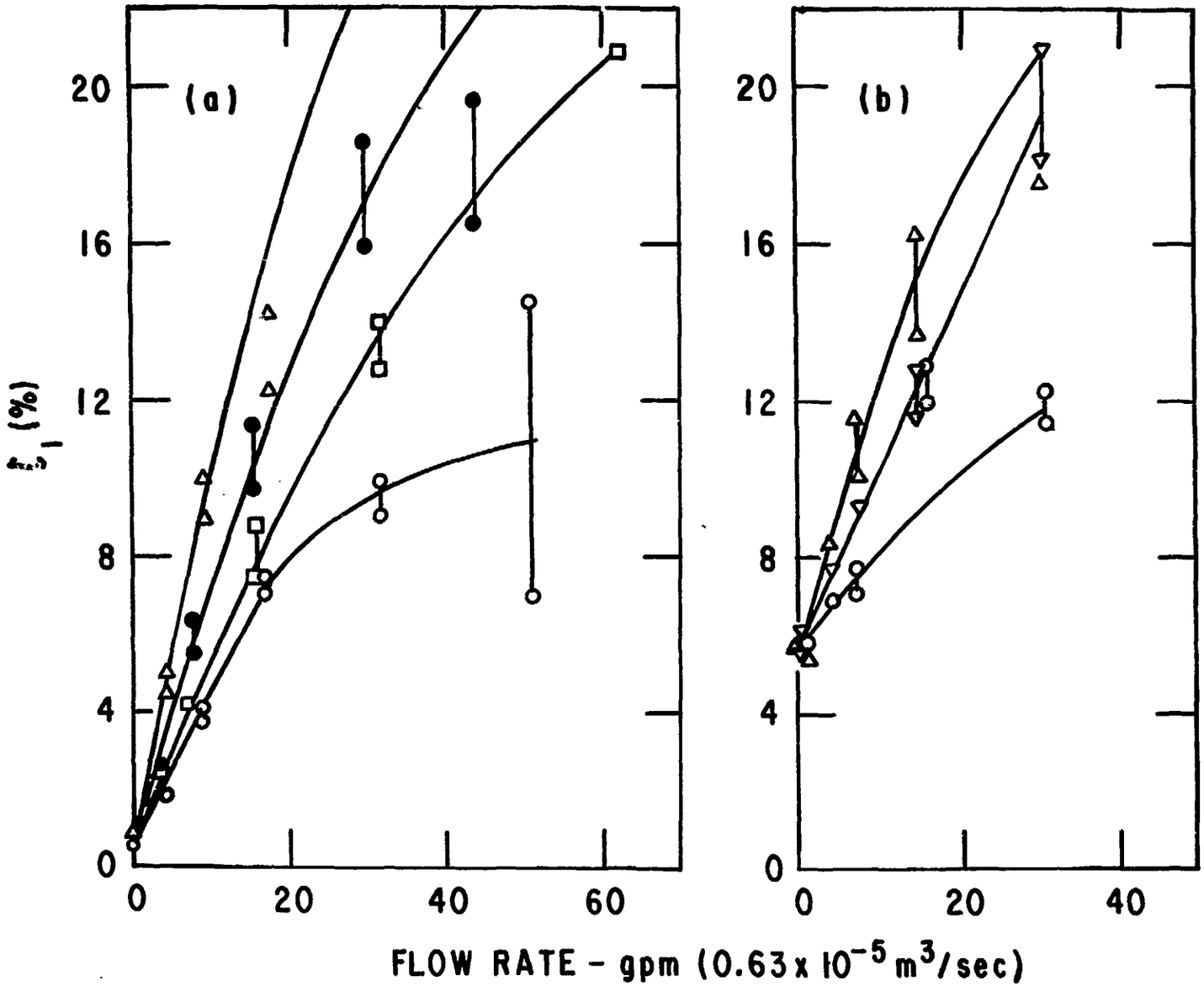

Fig. 10. Variation in First-mode Damping with Bottom-to-Top Flow for (a) H/D = 0.18 and (b) H/D = 1.09 where L/D = 0.28, ○ ; 0.46, □ ; 0.55, ▽ ; 0.64, ● ; 0.91, △

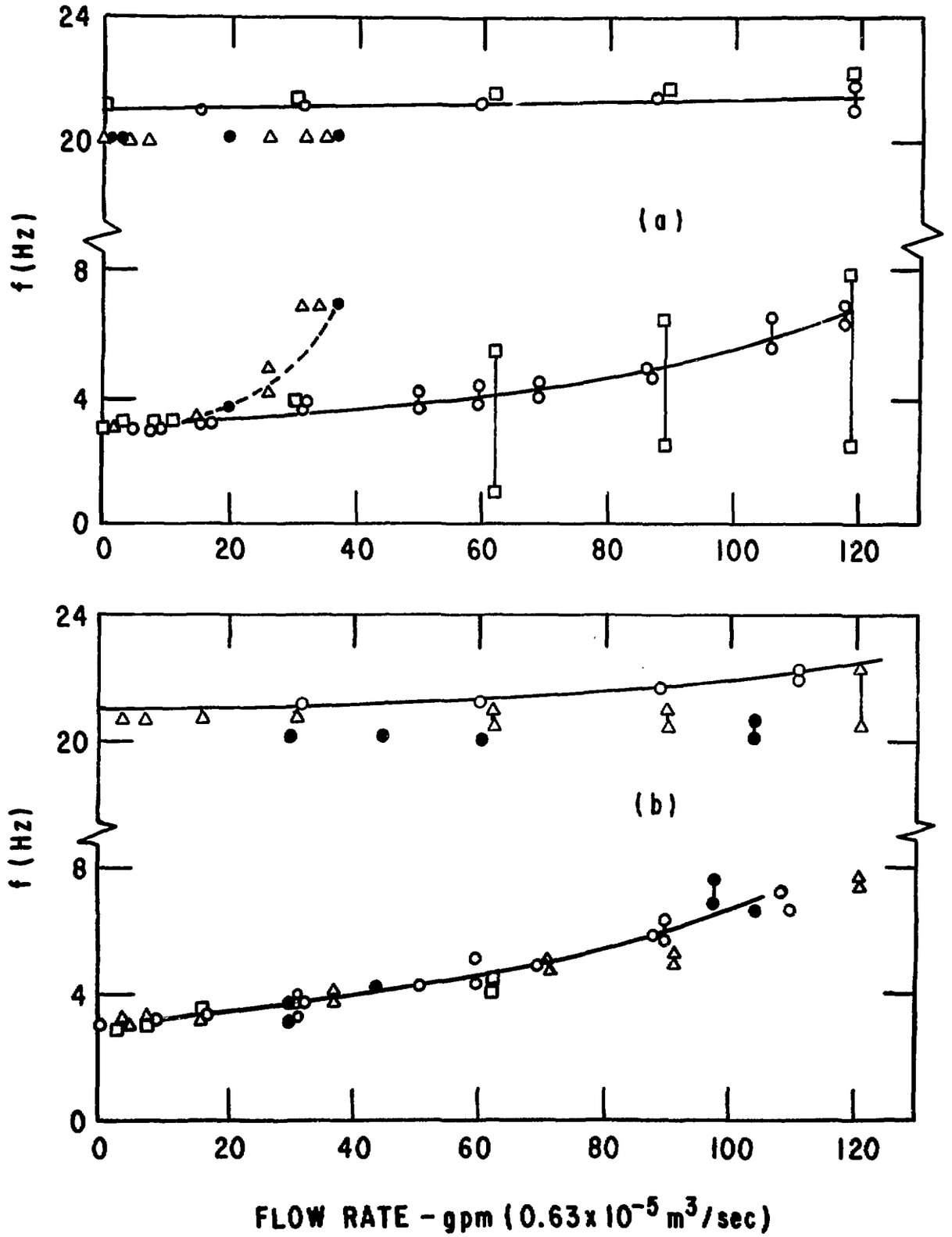

Fig. 11. Variation in First- and Second-mode Frequencies for (a) Top-to-Bottom Flow and (b) Bottom-to-Top Flow where H/D = 0.18 and L/D = 0.28, ○ ; 0.46, □ ; 0.55, ▽; 0.64, ● ; 0.91, △

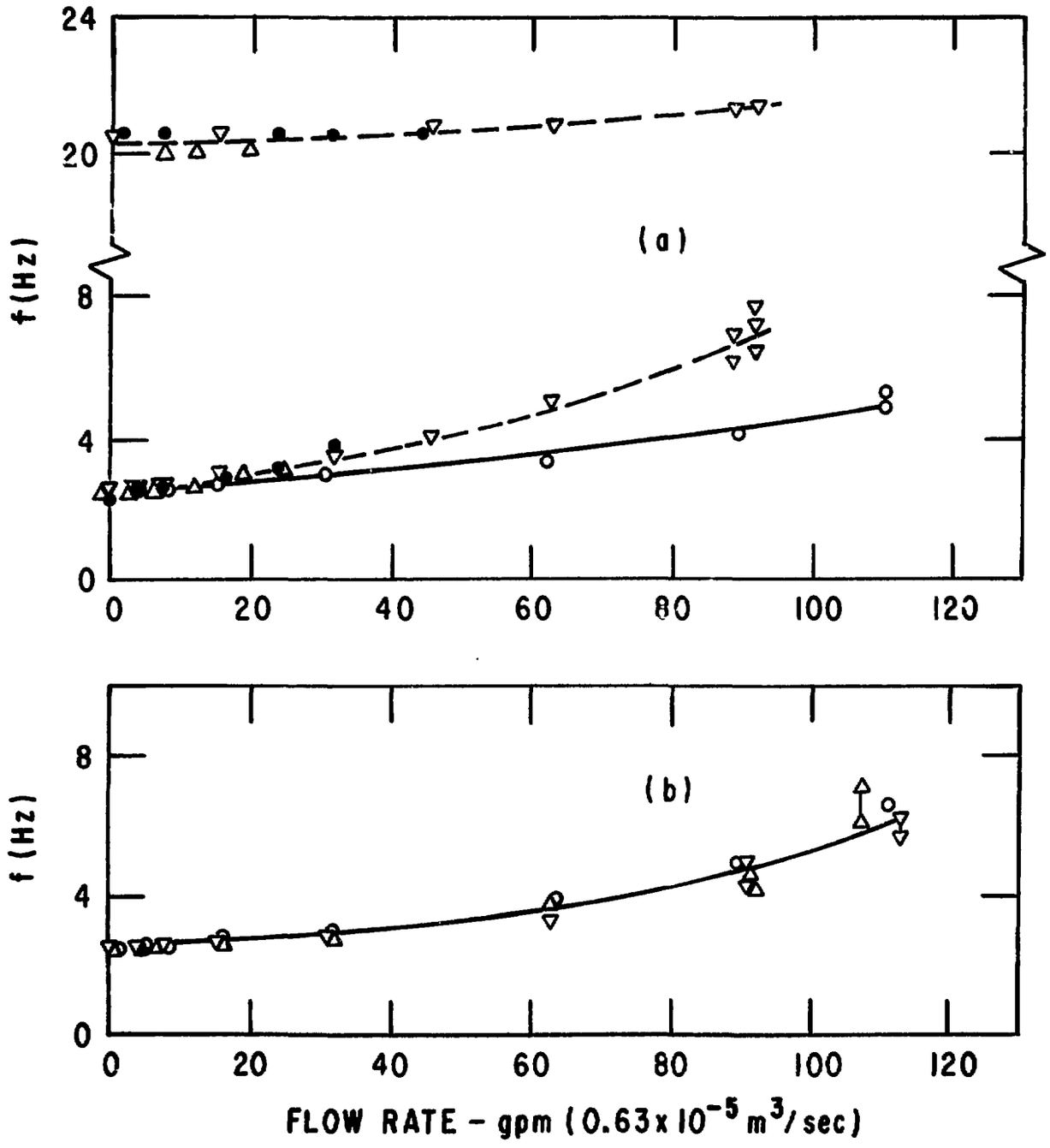

Fig. 12. Variation in First- and Second-mode Frequencies for (a) Top-to-Bottom Flow and (b) Bottom-to-Top Flow where H/D = 1.09 and L/D = 0.28, ○ ; 0.46, □ ; 0.55, ▽ ; 0.64, ● ; 0.91, △

IX. PRESSURE DIFFERENCE

The static pressure differences across the slip joint as a function of flowrate are shown in Fig. 13 for H/D = 0.18 and many engagement lengths. The data are for both an upstream and a downstream constriction, and even include some measurements where unstable motion occurred. Many data were taken for H/D = 1.09 and were found to be similar. This was expected, since the flow paths are not altered by changing structural damping. A flowrate up to 120 gpm (7.56×10^{-4} m^3/s) was attained, corresponding to a pressure difference of 42 $lb/in.^2$ (0.290 MPa). The average flow velocity through the constriction at the maximum flowrate was 55.7 ft/s (17 m/s). The pressure drop is nearly proportional to $(\text{flowrate})^2$ above 30 gpm (18.9×10^{-5} m^3/s), but closer to $(\text{flowrate})^{1.65}$ for smaller flowrates. The calibrated linear range of the turbine flowmeters F1-F3 was 7-70 gpm (4.4-44 m^3/s), which may be responsible for some of the variation at lower flowrates.

The most notable result from the pressure difference measurements was that they were nearly independent of the engagement length. In other words, the narrowest annulus formed by the constriction was the main source of pressure losses in the slip joint. Coupled with the previous observations that shorter engagement lengths weaken or suppress the instabilities, one can conclude the net forces and moments produced by the nonhomogeneous pressure field in the larger annulus between the tubes are an important part of the self-excitation mechanism. That is, both tubes must have afterbodies downstream from the constriction for unstable motion to occur.

X. ECCENTRICITY TEST

Having established that self-excited motion did not occur for concentric tubes with an upstream constriction and L/D <0.41 or with a downstream constriction, another flow test was run to assess the effects of lateral eccentricity. The borderline stable case of L/D $\simeq$ 0.41 and minimum first-mode damping, ζ_1 = 0.5%, was tested for the fully eccentric (tubes almost touching) case. This was considered the most likely case to cause instability or significant impacting. However, testing for flow in either direction showed that self-excitation did not occur no matter how much the flexible tube was perturbed. In fact, the gap between the tubes increased with increased flowrate. This static divergence was much more pronounced for an upstream constriction, in which case the tubes were nearly concentric at the maximum flowrate.

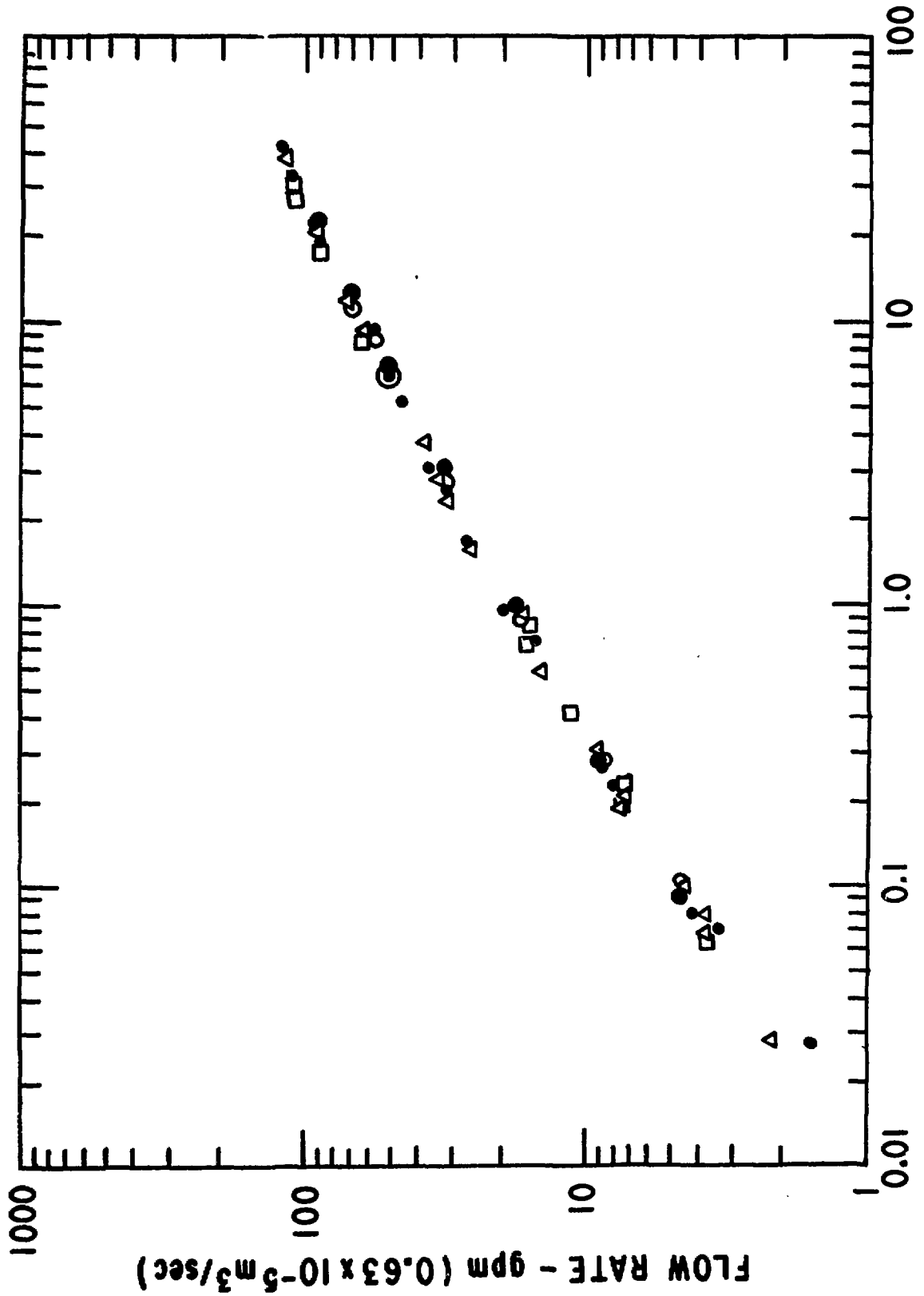

Fig. 13. Pressure Differences for Flow in Both Directions, H/D = 0.18, and L/D = 0.28, ○ ; 0.46, □ ; 0.55, ▽ ; 0.64, ● ; 0.91, △

XI. CONCLUSIONS

Significant flow-induced vibration has been observed for the much more flexible tube of a pair of two telescoping, cantilevered tubes concentrically engaged at their free ends by the slip joint shown as Case A in Fig. 4. The source of the excitation was flow through the slip joint from the top (outside) to the bottom (inside): flow past an upstream annular constriction. The undesirable motion, which often led to impacting between the tubes, was observed in the first or second vibration modes for many values of structural damping, engagement length, and flowrate. Measurement of total damping during flow testing showed that the translatory motion at the slip joint in the fundamental mode was a self-excited instability. Although damping in the second mode could not be controlled or monitored during flow testing, the rotational second-mode motion at the slip joint is believed to be a self-excited instability.

Unstable motion was more likely to occur for larger flowrates and engagement lengths, but smaller first-mode damping. Threshold values of flowrate and engagement length were determined below which no instabilities occurred. Also, threshold values of damping were identified above which no first-mode instabilities occurred. At threshold values of engagement length or damping the instabilities can be expected to be weak, and often disappear at higher flowrates. An instability map of critical flowrates for an upstream constriction versus engagement lengths and first-mode damping was determined (see Fig. 6) that can be used to define a design without unstable motion.

Testing with flow in the bottom (inside) to top (outside) direction, or flow past a downstream annular constriction, showed that no instabilities were present. Thus a simple design fix to avoid unstable motion is to use only downstream constrictions. If upstream constrictions must be used, instabilities can be suppressed by limiting the engagement length such that the annular region downstream from the constriction is nearly eliminated. In Fig. 6, the latter condition is achieved for $L < 2.25$ in. (57.2 mm) or $L/D < 0.41$.

The results cited above are for initially concentric tubes. Based on past experience [2], initial eccentricities can be expected to significantly effect critical flow velocities. However, a test for fully eccentric (almost touching) tubes showed no instabilities for $\zeta_1 = 0.5\%$ and $L/D > 0.41$ up to the maximum flowrate. More detailed testing with initial eccentricities is planned, but these preliminary results indicate that a design with $L/D < 0.41$ will be free from self-excitation.

ACKNOWLEDGMENTS

This work was performed under the sponsorship of the Office of Reactor Research and Technology, U. S. Department of Energy.

The author is grateful to Ed Bielick for the redesign and instrumentation of the test facility and to Roger Smith for his help in performing the flow tests. Also, the test program guidance and interpretation of results by Marty Wambsganss are much appreciated.

REFERENCES

1. M. P. Paidoussis, "Flow-Induced Vibration in Nuclear Reactors and Heat Exchangers: Practical Experiences and State of Knowledge," pp. 1-81 in Practical Experiences with Flow-Induced Vibrations (E. Naudascher and D. Rockwell, eds.), Springer-Verlag (1980).

2. T. M. Mulcahy, "Leakage Flow-Induced Vibrations of Reactor Components," The Shock and Vibration Digest 15(9), 11-18 (1983).

3. M. W. Parkin, "Flow-Induced Vibration Problems in Gas Cooled Reactors," pp. 126-136 in Practical Experiences with Flow-Induced Vibrations (E. Naudascher and D. Rockwell, eds.), Springer-Verlag, New York (1980).

4. T. M. Mulcahy, "Leakage Flow-Induced Vibration of a Tube-in-Tube Slip Joint," Paper D/9/P56 to be presented as part of the Symposium on Flow Induced Vibrations at the Winter ASME Meeting in New Orleans (1984).

5. T. M. Mulcahy, "Fluid Forces on Rods Vibrating in Finite Length Annular Regions," J. Appl. Mech. 102(2), 234-240 (June 1980).

Distribution for ANL-84-82

Internal:

A. Schriesheim
C. E. Till
R. S. Zeno
P. R. Huebotter
G. S. Rosenberg
M. W. Wambsganss
S. S. Chen
H. H. Chung
H. Halle
J. A. Jendrzejczyk
W. P. Lawrence
T. M. Mulcahy (75)
R. A. Valentin
S. K. Zussman
ANL Patent Dept.
ANL Contract File
ANL Libraries (2)
TIS Files (6)

External:

DOE-TIC, for distribution per UC-79k (126)
Manager, Chicago Operations Office, DOE
Director, Technology Management Div., DOE-CH
W. Frost, DOE-CH
Components Technology Division Review Committee:
P. Alexander, Flopetrol Johnston Schlumberger, Houston
D. J. Anthony, General Electric Co., San Jose
A. Bishop, U. of Pittsburgh
B. A. Boley, Northwestern U.
F. W. Buckman, Delian Corporation, Monroeville, PA
R. Cohen, Purdue U.
J. Weisman, U. of Cincinnati